# Sequential Plasma-Activated Bonding Mechanism of Silicon/Silicon Wafers

Matiar M. R. Howlader, G. Kagami, Sang Ho Lee, Jinguo G. Wang, Moon J. Kim, and Akira Yamauchi

*Abstract*—To investigate the sequentially plasma-activated bonding (SPAB) mechanism of silicon/silicon wafers, the surface hydrophilicity, and the interface voids, nanostructures and chemical compositions that control the bonding quality, such as bonding strength, have been observed. Although the sequentially plasma-activated surfaces are hydrophilic, the SPAB mechanism is not identical to the hydrophilic bonding. SPAB shows high bonding strength at room temperature and water rearrangement below 150 °C, which removes the water from the interface to the bulk. This results in a thinner amorphous silicon oxide layer at the interface. Further heating of the bonded wafers desorbs water from the bulk. The heating at 225 °C starts producing hillocks at the interface, which turn into voids at temperatures above 400 °C for absorbing the hydrogen gas produced from the desorbed water at the interface. The new and bigger voids are due to the hydrogen gas at 600 °C and start accumulating at 800 °C, resulting in bubbles caused by the accumulation of voids at the preferential sites. No nitrogen exists either in silicon or in the amorphous $SiO_2$ layer at the interface. The $Si-L_{2,3}$ edges from the amorphous silicon oxide at the bonded interface are identical to those of the standard $SiO_2$.             [2009-0253]

*Index Terms*—Amorphous silicon oxide layer, electron energy loss spectroscopy (EELS), interfacial nanostructure, sequentially plasma-activated bonding (SPAB) mechanism, voids formation, water contact angle.

## I. INTRODUCTION

**W**AFER direct bonding (WDB) joins two mirror-polished surfaces without using any intermediate layers. Due to its simplicity, this technique has been widely utilized to bond silicon wafers for microelectromechanical systems (MEMS), optoelectronic devices, and fabrication of silicon-on-insulator (SOI) structures [1], [2]. One of the approaches to achieve such WDB of silicon wafers is to prepare hydrophilic surfaces using wet chemicals, such as RCA1 ($NH_4OH : H_2O_2 :$

$H_2O = 1 : 1 : 5$) and RCA2 ($HCl : H_2O_2 : H_2O = 1 : 1 : 6$). The chemical cleaning processes remove organics, metals, and alkaline contaminants. These hydrophilic surfaces bond due to the van der Waals attraction through hydrogen bonds between the $OH^-$ terminated surfaces. Thermal heating at elevated temperatures as high as 1000 °C is required to obtain strong Si-O-Si bonds across the interface [1]–[3]. In fact, temperature-sensitive MEMS devices, such as an image sensor, are not compatible to heating at such high temperatures [4].

To reduce the bonding temperature, plasma-activated bonding processes, such as reactive ion etching (RIE) [5]–[7], microwave (MW) [8], inductively coupled plasma [9], and ultraviolet [10] radiation plasma using different atmospheres, such as argon, oxygen, nitrogen, and hydrogen gases, have been reported. The plasma-assisted bonding processes utilize heating at temperatures as low as 200 °C–300 °C to obtain high bonding strength. However, during the heating process, voids are formed at the bonded interface of silicon/silicon [5], [7], [9], [11]. This is due to the plasma-induced defects and the hydrogen gas caused by reactions between water molecules and silicon. Plasma-assisted bonding methods have been demonstrated in the wafer scale packaging of MEMS devices [12]. However, in practical applications, metalized layers and circuits on wafers may be destroyed even at these low bonding temperatures. In addition, materials with high lattice and thermal mismatch, such as silicon and lithium niobate, fracture at these low (i.e., 200 °C) temperatures [13]. Therefore, the integration of temperature-sensitive devices and materials with high lattice and thermal mismatch requires room-temperature plasma bonding.

A room-temperature plasma bonding process has been developed utilizing the physical sputtering of oxygen ($O_2$) RIE and the chemical reactivity of nitrogen ($N_2$) MW radicals on the same surface one after another. This is a two-step surface activation method called the sequential plasma-activated bonding (SPAB) process [14], [15]. The mating surfaces are activated with oxygen RIE plasma followed by nitrogen radical cleaning in a low vacuum and bonded in clean room atmosphere with hand-applied pressure. The advantage of this method is the bonding capability of delicate microelectromechanical systems (MEMS) and temperature-sensitive diverse circuits, components, and devices at room temperature. In addition, the bonding strength of silicon/silicon as high as 25 MPa was achieved in SPAB at room temperature, which was equivalent/higher than that in the hydrophilic and hydrophobic bonding processes at high temperature ($\sim$ 1000 °C) [14]–[16]. While SPAB has been evaluated for diverse applications, such as hermetic sealing using silicon/glass [17] and

M. M. R. Howlader is with the Electrical and Computer Engineering Department, McMaster University, Hamilton, ON L8S 4L7, Canada (e-mail: mrhowlader@ece.mcmaster.ca).

G. Kagami is with Shinko Seiki Company Ltd., Kobe-City 651-2271, Japan (e-mail: g-kagami@shinko-seiki.com).

S. H. Lee, J. G. Wang, and M. J. Kim are with the Department of Materials Science and Engineering, University of Texas at Dallas, Richardson, TX 75083 USA (e-mail: shlee@utdallas.edu; jinguo.wang@utdallas.edu; moonkim@utdallas.edu).

A. Yamauchi is with Bondtech Company Ltd., Kyoto 611-0033, Japan (e-mail: akira_0421@msh.biglobe.ne.jp).
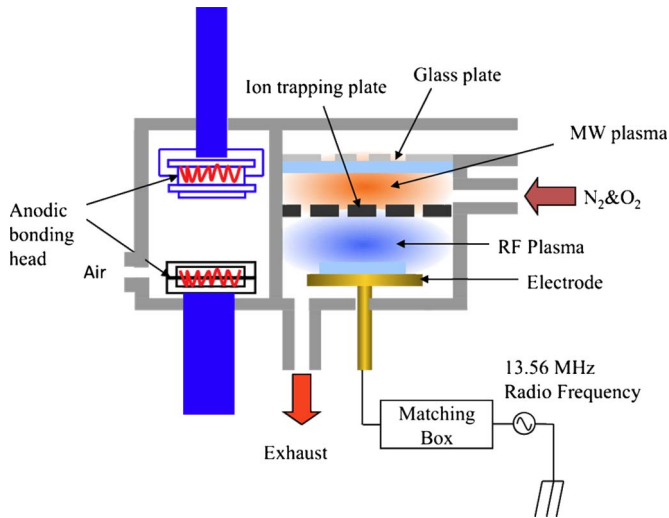
Fig. 1. Schematic of the HPB system.

glass/glass [16] bonding wafers with microcavity bonding at room temperature, most of the studies hypothetically explained the bonding mechanism of SPAB. For example, $O_2$ RIE plasma activation followed by nitrogen radical treatment increased the bonding strength of silicon/glass and glass/glass, which was believed to be due to the diffusion of absorbing water into bulk silicon [16], [17].

Similar to other plasma-assisted bonding methods, one of the issues in SPAB is the voids or unbonded regions at the interface. Voids control the reliability of the bonded interface, such as bonding strength, hermeticity, or electrical properties [18]. In practical applications, such as smart-cut process, bonded specimens go through up to 600 °C heating steps to fabricate the SOI substrate [19]. Hence, the evolution of void formation at the bonded interface with different heating temperature needs to be investigated.

Although heat treatment of silicon/silicon in hydrophilic and other plasma-assisted bonding increased the bonding strength, heating reduced the bonding strength in SPAB [20]. One of the reasons for this temperature-dependent discrepant behavior in SPAB is the combined effect of surface hydrophilicity and reactivity. It controls the bonded interface properties, such as bonding strength and voids [18]. Surface reactivity influences hydrophilicity, which can be directly determined through measurement of contact angle of a drop of distilled water on the surface. To observe the hydrophilicity of the sequentially plasma-activated surfaces, the contact angle measurements with different plasma parameters need to be analyzed.

This paper reports the bonding mechanism of the sequentially plasma-activated silicon/silicon bonded wafers through the investigation of surface hydrophilicity, heating influence on interface, and compositional analysis of the interface.

## II. EXPERIMENTAL

P-type single-side mirror-polished CZ-grown (100) silicon wafers with a thickness of 500 $\mu$m were used for the experiments. The wafer-level hybrid plasma bonding (HPB) system, as shown in Fig. 1, was used for the bonding experiments.

The HPB system accommodates up to 200-mm-size wafers. It consists of plasma activation and anodic bonding chambers. The plasma activation chamber was only used for bonding. The plasma activation chamber is equipped with RIE and MW plasma sources. The plasma activation chamber is separated into top and bottom compartments by an ion trapping metallic plate. The metallic plate has holes of 1 mm, which trap charged ions. The RIE and MW plasma were sequentially generated using $O_2$ and $N_2$ gases, respectively. The RIE and MW plasma generate at the bottom and top compartments of the chamber, respectively. Therefore, the MW plasma generates electrically neutral ions.

For sequential plasma activation, first, oxygen radio-frequency plasma was shot at the wafers with a frequency of 13.85 MHz, followed by nitrogen MW plasma with a frequency of 2.45 GHz. Commercially available wafers were used for surface activation. Prior to or after the surface activation, the wafers were not dipped in wet chemical and/or water. After surface activation, the wafers were contacted under hand-applied pressure outside the vacuum chamber in a class 10 000 clean room under ambient conditions. Finally, the contacted wafers were rolled under a 100-kg force without heating to remove trapped air across the interface. Table I shows the plasma-generating conditions and the surface activation parameters for the different experiments.

Five sets of experiments were conducted using the (100) silicon wafers, as shown in Table I. For tensile strength measurements, the bonded specimens were diced into $10 \times 10$ mm$^2$ pieces. The diced pieces were glued with copper jigs, and the tensile strength was measured using a tensile tester from Instron. Contact angle measurements were completed using equipment from Kyowa Interface Science Company, Ltd. (model #DM300) to measure the angle between the surface and a droplet of water placed on the wafer surface. The quantity of water used for contact angle measurement was about 1 $\mu$L. The nanostructural bonded interface, as well as its electron energy loss spectroscopy (EELS) measurements, was done using high-resolution transmission electron microscopy (HRTEM) (JEOL model #2010) to investigate the thickness of the interfacial layer and the elemental composition at the bonded interface. The specimens for HRTEM observations were heated for 1 h in air at different temperatures up to 225 °C. Further heated specimens at temperatures up to 900 °C were investigated using infrared transmission images that link between nano-structures observed by HRTEM to microstructures of the bonded interface.

## III. RESULTS AND DISCUSSION

### A. Temperature Dependence of Bonding Strength

Fig. 2 shows the bonding strength of silicon/silicon in SPAB and the hydrophilic bonding [21] methods as a function of heating temperature. In hydrophilic bonding, the bonding strength increased with the increase in heating temperatures at different slopes. The temperature dependence of the bonding strength in the hydrophilic method indicates water re-arrangements (i.e., diffusion and absorption) at different heating

TABLE I
EXPERIMENTAL CONDITIONS OF PLASMA PARAMETERS IN THE SPAB PROCESS

| Experiments | $O_2$ RIE Plasma | | | $N_2$ MW Radicals | | | Heating (°C) |
|---|---|---|---|---|---|---|---|
| | Power (W) | Time (s) | Pressure (Pa) | Power (W) | Time (s) | Pressure (Pa) | |
| Heating temperature vs. tensile strength | 200 | 60 | 100 | 2000 | 30 | 100 | 150-600 |
| RIE Power vs. Contact angle | 100 200 300 400 | 60 | 100 | 2000 | 30 | 100 | No |
| RIE Pressure vs. Contact angle | 300 | 60 | 40 60 80 100 | 2000 | 30 | 100 | No |
| RIE Time vs. Contact angle | 300 | 30 60 120 300 | 40,100 | 2000 | 30 | 100 | No |
| HRTEM | 50 | 15 | 60 | 2500 | 30 | 60 | 50- 225 |
| IR transmission | 200 | 60 | 50 | 2500 | 30 | 60 | 200-900 |
| EELS | 200 | 60 | 100 | 2000 | 30 | 100 | 200-600 |
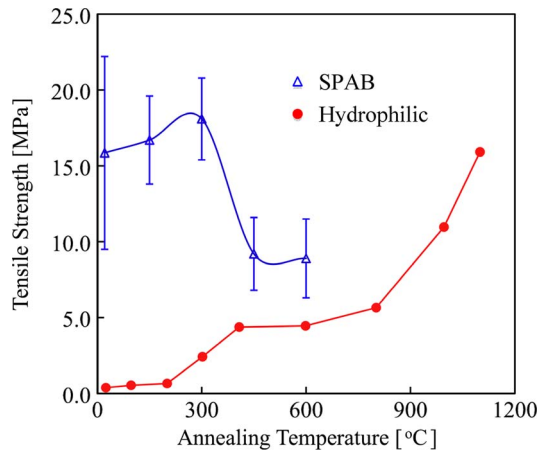


Fig. 2. Bonding strength of silicon/silicon in SPAB compared with hydrophilic bonding strength [21] as a function of heating temperature.

temperatures that form siloxane bonds at the interface [18]. The bonding strength in SPAB at room temperature was identical to that in hydrophilic bonding at 1100 °C (i.e., 16 MPa). In SPAB, the bonding strength at room temperature was not significantly increased after heating at 300 °C (i.e., 18.1 MPa). In fact, the bonding strength was considerably decreased with the increase in the heating temperature, but still the bonding strength at 600 °C was higher than that at 800 °C in hydrophilic bonding. This result indicates that although OH⁻ molecules terminate the bonding surfaces in both SPAB and hydrophilic bonding methods, the bonding mechanisms are different.

## B. Surface Hydrophilicity

To understand the surface hydrophilicity in sequential plasma activation, the water contact angle measurements were investi-

gated with different plasma parameters, such as $O_2$ RIE power, time, and pressure, and storage time after activation. Table II summarizes the average contact angles as a function of $O_2$ RIE plasma power, pressure, and time. The contact angle before surface activation was about 22°; it jumped to around 60° after activation at different plasma processing parameters. An increasing trend of contact angle with increasing RIE power was observed. The standard deviation at higher power may indicate an increased amount of surface roughness [22]. The rough surface has a higher contact angle compared with that of the smooth surface [23]. On the other hand, the contact angles were not significantly changed with increasing RIE activation time. The drop of contact angle at 60-s RIE time was due to the reduced surface roughness [20]. The contact angles were proportionately increased with RIE pressures except at 100 Pa. The increase in surface roughness with the increase in $O_2$ RIE pressure has been reported [20]. High pressure in $O_2$ RIE results in excess OH⁻ molecules, which has a dominant role over the surface roughness. Therefore, the reduction of contact angle at 100-Pa $O_2$ RIE pressure was attributed to the excess of OH⁻ molecules on the surface. A comparison among these results indicates that the RIE power and pressure dominate the hydrophilicity of silicon surface compared with the RIE time.

The activated surfaces have hydrophilic layers that may be changed due to exposure in air. The rate of change of the contact angle refers to the surface reactivity. This represents reactions between the large numbers of dangling bonds terminated on the plasma-activated surfaces and the hydroxyl molecules from the surrounding environment. Since the plasma-activated bonding is performed in air, the measurement of contact angle as a function of elapsing time after surface activation is important to clarify the surface reactivity. Fig. 3 shows the elapsed time dependence of contact angle of the silicon surface activated using a 300-W $O_2$ RIE plasma at 100 Pa for 60 s followed by a

TABLE II
AVERAGE CONTACT ANGLES OF A DROP OF DEIONIZED (DI) WATER ON Si WAFER SURFACE WITH DIFFERENT SURFACE TREATMENT CONDITIONS

| O$_2$ RIE Plasma | | | N$_2$ MW Radicals | | | Contact |
|---|---|---|---|---|---|---|
| Power (W) | Time (s) | Pressure (Pa) | Power (W) | Time (s) | Pressure (Pa) | angle (deg) |
| 100 | 60 | 100 | 2000 | 30 | 100 | 60.0±1.1 |
| 200 | | | | | | 60.7±1.6 |
| 300 | | | | | | 61.2±0.5 |
| 400 | | | | | | 61.3±2.3 |
| 300 | 60 | 40 | 2000 | 30 | 100 | 56.7±0.5 |
| | | 60 | | | | 60.4±1.0 |
| | | 80 | | | | 64.3±0.5 |
| | | 100 | | | | 61.2±0.2 |
| 300 | 30 | 40 | 2000 | 30 | 100 | 60.0±0.8 |
| | 60 | | | | | 56.7±0.5 |
| | 120 | | | | | 60.9±0.7 |
| | 300 | | | | | 62.3±1.2 |
| 300 | 30 | 100 | 2000 | 30 | 100 | 63.7±0.5 |
| | 60 | | | | | 61.2±0.5 |
| | 120 | | | | | 64.7±0.3 |
| | 300 | | | | | 60.3±0.5 |
| Without activation | | | | | | 22.0±0.1 |

2000-W nitrogen radical plasma at 100 Pa for 30 s. The value at zero time in the graph is the sequentially activated surface. The contact angle exponentially decreased with elapsed time after surface activation. After 30 min leaving in air, the contact angle returned back almost close to the value before activation. This indicates that the sequentially treated surfaces are highly reactive. This reduction was attributed to the deposition of hydroxyl molecules and trapping particles from clean room atmosphere to the surface. The standard deviations of the contact angles reduced with elapsed time after surface activation. Again, this high reactivity supports the deposition of hydroxyl molecules and trapping particles on the surface. The greater the elapsed time, the greater the deposition of hydroxyl molecules, resulting in reduced contact angle. An identical behavior of the contact angles of the Si surface treated with O$_2$ RIE plasma has been observed [24]. However, the absolute value of the contact angle in the O$_2$ RIE plasma was higher than that in SPAB. These results indicate that SPAB should be done immediately after surface activation. This finding is inconsistent with the hydrophilicity of plasma-activated (100-W O$_2$ RIE for 5–10 s) silicon specimen, which remained hydrophilic in excess of 150 h [25]. In fact, the reported contacted angle after 150 h was 14.6°, which was even lower than that before surface activation (22°) in this paper. The absolute value of the contact angle in the sequentially activated (O$_2$ RIE 60 s and N$_2$ radicals 30 s) silicon surface was 61.2°. In addition, the contact angle was 27° after storing the sequentially activated surface for 30 min in air (Fig. 3). In [26], the contact angle of the silicon surface activated using a 100-W O$_2$ RIE for 60 s was 10.7°. This reported contact angle was measured after 2 h from surface activation. Therefore, the results show that the combined effect of O$_2$ RIE and N$_2$ radicals (sequential activation) improved not only the hydrophilicity compared with other plasma activation but also the reactivity of the surfaces. These surfaces are responsible for an enhanced bonding strength without heating. This is consistent with the bonding energy, which increased from 0.05 to 2.3 J/m$^2$ after storage at room temperature for 24 h [27].
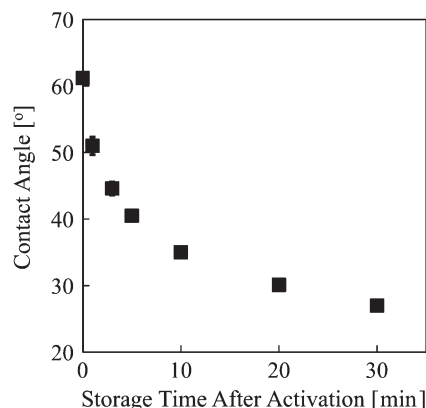


Fig. 3. Contact angles of SPAB with elapsed time after activation. The sequential activation was done using a 300-W O$_2$ RIE plasma at 100 Pa for 60 s followed by a 2000-W N$_2$ MW radical plasma at 100 Pa for 30 s.

## C. Low-Temperature Heating Effect on Interfacial Nanostructure

To clarify whether the diffusion of OH molecules [17] from the interface into bulk silicon causes high bonding strength of silicon/silicon in SPAB, the silicon/silicon interfaces were extensively investigated after heating at low temperatures. Fig. 4 shows the HRTEM interface images of the silicon/silicon wafers bonded by SPAB heating at 50 °C, 100 °C, 150 °C, and 225 °C for 1 h in air. The bonding conditions for the specimens used were oxygen RIE plasma time of 15 s at 60 Pa and nitrogen radical time of 30 s at 60 Pa. HRTEM images showed intermediate amorphous layers across all the interfaces. The thicknesses of the amorphous layer after heating at 50 °C, 100 °C, 150 °C, and 225 °C were 3.8, 3.4, 2.8, and 3.3 nm, respectively, as summarized in Table III. The decreased thickness of the amorphous layer from 50 °C to 150 °C indicates absorption of hydroxyl molecules from the interface to the bulk of silicon. At 225 °C, the increased thickness of the amorphous layer compared with that in 150 °C attributes to the desorption of hydroxyl molecules from the bulk of silicon to the interface.
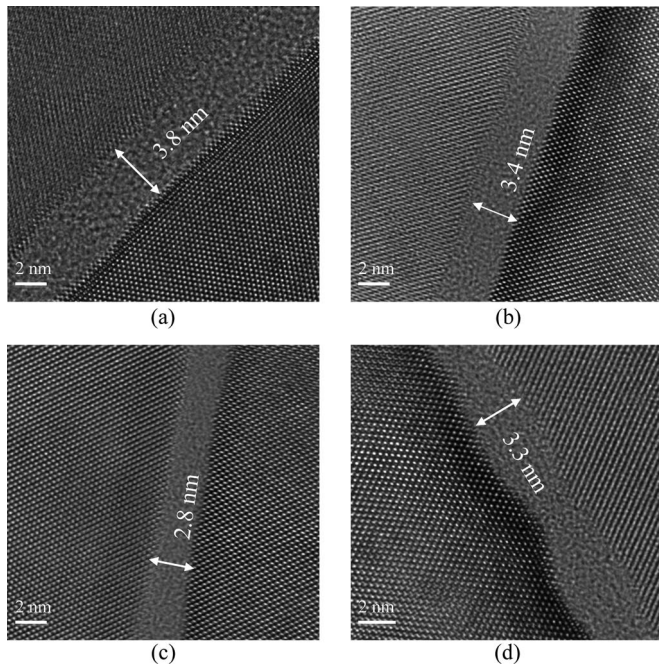
Fig. 4.   HRTEM images of the silicon/silicon interfaces created by SPAB that were heated at (a) 50 °C, (b) 100 °C, (c) 150 °C, and (d) 225 °C for 1 h in air. The sequential activation includes a 50-W oxygen RIE plasma with time of 15 s at 60 Pa and a 2500-W MW nitrogen radical with time of 30 s at 60 Pa.

The heating at 225 °C starts producing hillocks at the interface, which may turn into voids at higher temperatures to absorb the gas produced from the desorbed water at the interface. The heating at higher temperature (i.e., 600 °C) increased the thickness of the amorphous layer compared with the room temperature [15]. In addition, the bonding strength was severely reduced at 600 °C due to the brittle nature of the amorphous oxide layers and excess voids. The finding of this paper combined with the previous one may indicate water absorption from the interface to the bulk and water desorption from the bulk of silicon to the interface, depending on the temperature range.

Although the HRTEM images at further high temperatures may allow insight into the phenomena of the amorphous layer, the IR images at different temperatures give a wide level understanding important to understanding the bonding mechanism. Water absorbs by silicon and then desorbs water into bulk silicon. This process may generate interfacial silicon oxides with unprecedented phenomena at macro scale, which can be investigated by taking the IR images of the interfaces before and after heating. The reactivity measurements at the bonded interface of two oxygen-plasma-treated SiN layers were examined using a bonded structure from which one of the GaAs wafers is removed. The SiN layers were deposited on GaAs wafers and bonded after treating with oxygen plasma. The heating of the bonded structures at 150 °C and 300 °C increased the interfacial thickness and density of $SiO_x$ [28].

### D. Heating Influence on Interfacial Voids

To extend the growth mechanism of $SiO_2$ at the bonded interface in the sequential activation process under heating at high temperature, the specimen prepared by a 200-W RIE power at 60 s and 50 Pa followed by 2500-W MW nitrogen radicals at 30 s and 60 Pa was heated for 2 h in air. Fig. 5 shows the IR images of silicon/silicon interfaces heated from room temperature to 800 °C with 200 °C steps. It also includes the result for 900 °C. The IR images were taken for the same bonded specimen heated at different temperatures. At room temperature, a number of processing particles and induced voids appeared across the prepared interface. From 200 °C to 400 °C, a few voids were newly generated, and some preexisting voids grew larger. At 600 °C, the size, shape, and quantity of the voids were significantly changed, and an abrupt change was observed. The abrupt change of the size and shape of the voids at 600 °C may be attributed to the viscous flow of hydrogen gases across the interface [18], [20]. At 600 °C, the voids became bubbles. At 800 °C, new shapes of the bubbles were defined when compared with the voids at 900 °C. The shapes and sizes of the bubbles and voids cannot further be changed with increased temperature due to the strong bonding of the surrounding area of the bubbles and voids.

The growth mechanism of $SiO_2$ observed through IR observations can be explained in conjunction with the HRTEM observation. The thickness of the $SiO_2$ at 225 °C was 2.8 nm. At this condition, the IR image shows distinct appearance Newton rings in voids compared with RT. The thickness reduction at 225 °C is due to the appearance of those Newton rings. In other words, the water was desorbed from the bulk, consistent to the nanostructural observation at 225 °C. The water from the bulk starts causing new voids. At 600 °C, the viscous flow due to gas generation from water generates bubbles. The height of the $SiO_2$ at the interface supports the viscous flow. Further heating in 900 °C results in increase in the $SiO_2$ thickness.

### E. High-Temperature Heating Effect on Interfacial Nanostructure and EELS Measurements

Transmission electron microscopy (TEM) cross-sectional samples were prepared by standard sample preparation techniques with low-energy ion milling as the final step. HRTEM, high angle annular dark field (HAADF)-scanning tunneling electron microscope (STEM), and EELS were performed using a field-emission TEM (JEOL 2100F, $Cs = 0.50$ mm) in conjunction with a Gatan Enfina 1000 spectrometer operating at 200 kV. The energy resolution was about 1.0 eV. The typical probe conditions for EELS used in this paper consisted of 1.0-nm diameter probe in TEM condition and a ~0.3-nm diameter probe with a convergence semiangle of 14 mrad in STEM condition. Core-loss EELS spectra of N-K, $Si-L_{2,3}$, and O-K were recorded. Fig. 6(a) and (b) shows the HRTEM images of the silicon/silicon-bonded interface that was processed by a 200-W $O_2$ RIE plasma for 60 s at 100 Pa followed by a 2000-W $N_2$ MW plasma for 30 s at 100 Pa before and after heating. This specimen was annealed first at a temperature of 200 °C, then at 400 °C, and finally at 600 °C. At all three temperatures, the specimen was annealed for 4 h in the air with a ramping rate of 200 °C/h. The HRTEM images of the bonded interface showed that the interfacial amorphous layer of the specimen increased from ~4.8 to ~13 nm. This is much higher than that of the specimen annealed at 225 °C.

TABLE III
AMORPHOUS LAYER THICKNESSES AT THE INTERFACES OF SILICON WAFERS BONDED BY THE SPAB PROCESS AFTER HEATING AT LOW
TEMPERATURES FOR 1 H IN AIR. IN THE SPAB PROCESS, THE SURFACE OF WAFER WAS ACTIVATED BY 50-W $O_2$ RIE PLASMA
FOR 15 s AT 60 Pa FOLLOWED BY 2500-W $N_2$ MW RADICALS FOR 30 s AT 60 Pa

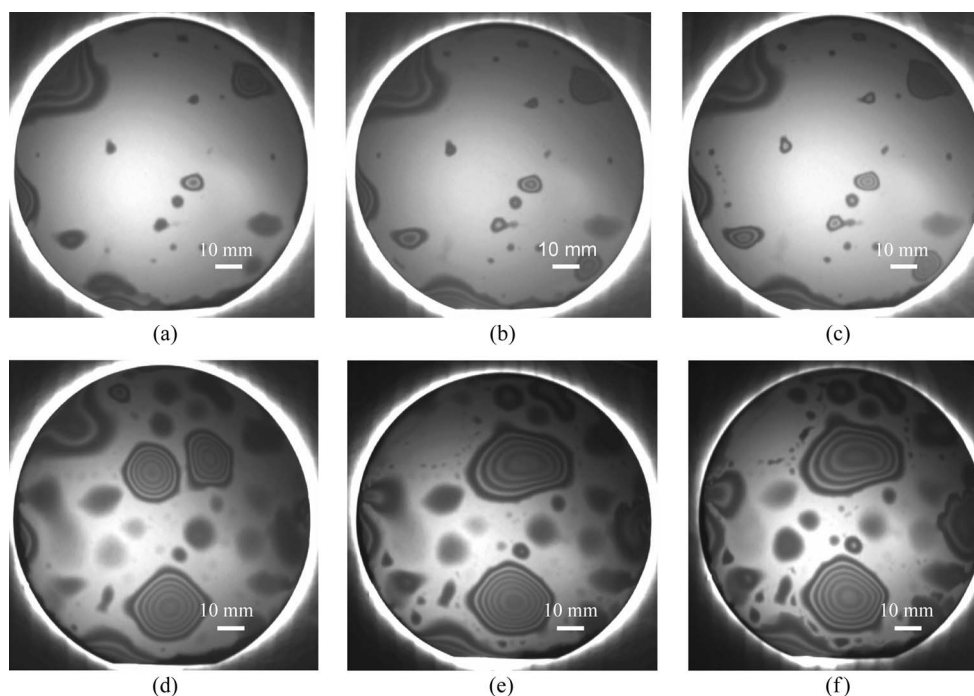| Heating temperature (°C) | Amorphous layer thickness (nm) | Comments |
|---|---|---|
| 50 | 3.8 | |
| 100 | 3.4 | ⇩ |
| 150 | 2.8 | |
| 225 | 3.3 | Hillocks |



Fig. 5. Infrared transmission images of silicon/silicon interfaces annealed up to 800 °C with 200 °C steps and 900 °C. The sequential activation includes a 200-W oxygen RIE plasma with time of 60 s at 50 Pa and a 2500-W MW nitrogen radical with time of 30 s at 60 Pa. (a) RT. (b) 200 °C. (c) 400 °C. (d) 600 °C. (e) 800 °C. (f) 900 °C.

The increased height of the amorphous layers attributes to the viscous flow of interface oxide at 600 °C [20]. Fig. 6(c) shows the HAADF image of this specimen after heating. Fig. 6(d) shows a low-loss EELS profile over an energy range from 5 to 50 eV. Spectra have been recorded at 0.5-nm intervals along the 13-nm line trace shown in Fig. 6(c). All spectra have been calibrated to the zero loss peak (ZLP) and deconvulated to remove multiple scattering influences. The spectrum for silicon reduces with approach to the interface and becomes constant with the lowest amplitudes through the interface. The spectrum for oxide increased with approach to the interface and becomes constant with the highest amplitudes through the interface.

The role of nitrogen radicals on the bonded interface of the annealed specimen at 600 °C was investigated using EELS measurements. Fig. 7(a) shows the EELS for the detection of elements at the bonded interface. Elemental detection at the bonded interface using the EELS spectra provides such insights that were done at a, b, and c points marked on the image in Fig. 6(c). There was no nitrogen detected in all the spectra [29]. The O-K edges at 540–560 eV were observed at the amorphous oxide layer of the interface. Further analysis of the Si-$L_{2,3}$

of amorphous silicon oxide compared with standard Si and $SiO_2$ provides the characteristic behavior of amorphous layer at the interface. Fig. 7(b) shows the Si-$L_{2,3}$ edges from the interfacial amorphous oxide layer compared with the standard Si and $SiO_2$. The Si-$L_{2,3}$ edges from the amorphous $SiO_2$ were identical with that of the standard $SiO_2$ at the bonded interface. This implies that $SiO_2$ is present at the interface. The scanning for the elemental distribution of Si and O across the interface also showed the proportional distribution, which is consistent with that of the result of amorphous $SiO_2$ at the interface.

Before heating, the role of $N_2$ MW radicals in SPAB has been investigated. Although there is no nitrogen detected either in bulk silicon or amorphous $SiO_2$ layer at the interface, the bonding strength in SPAB is higher than that in the $O_2$ RIE plasma-activated bonding at room temperature [30]. The improved bonding strength was due to the $N_2$ MW radical treatment after the $O_2$ RIE plasma activation. The interfacial amorphous silicon oxide was oxygen deficient. This is due to the existence of $SiO_xN_y$ (beyond EELS detection limit) at the sequentially plasma treated surfaces [14], [15], [20]. These surfaces are hydrophilic and highly reactive. When these surfaces

(a)                                    (b)
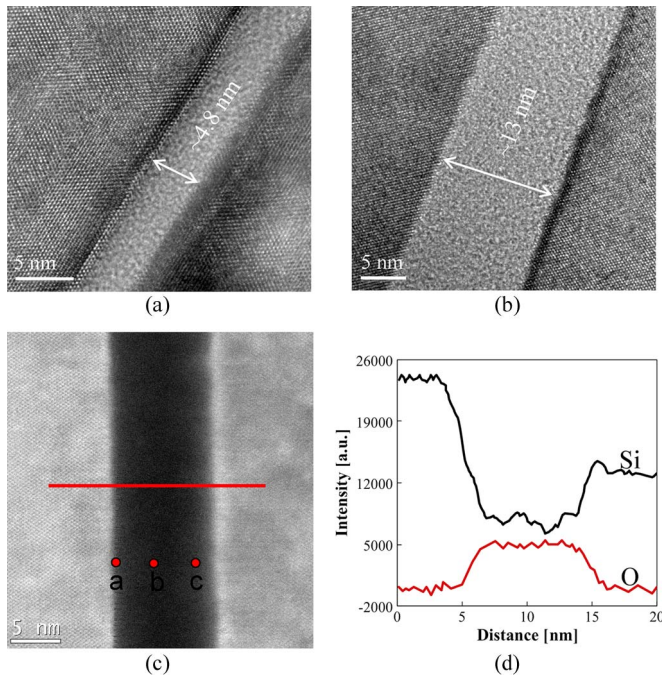
(c)                                    (d)

Fig. 6.   (a) HRTEM images of Si/Si sequential plasma-activated bonded interfaces of specimen before heating, (b) after heating at 600 °C, (c) STEM image of silicon/silicon-bonded interface recorded with a HAADF detector. Horizontal line indicates EELS line scan position. (d) STEM-EELS spectrum imaging line profile across the interface amorphous layer. The specimen for the STEM image were processed by a 200-W $O_2$ RIE plasma for 60 s at 100 Pa followed by a 2000-W $N_2$ MW plasma for 30 s at 100 Pa. The specimen was annealed first at a temperature of 200 °C, then at 400 °C, and finally at 600 °C. At all three temperatures, the specimen was annealed for 4 h in air with a ramping rate of 200 °C/h.
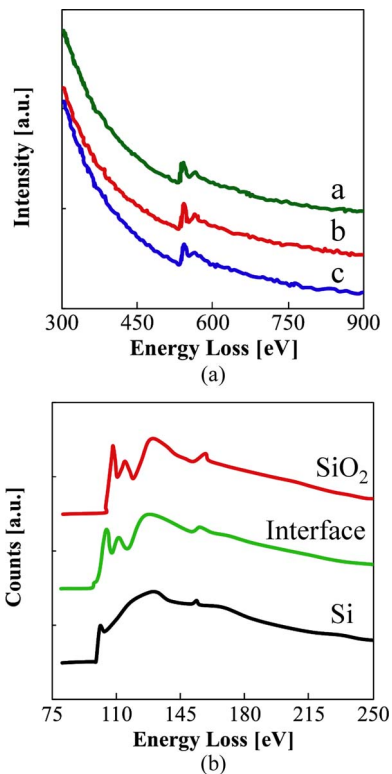


(a)

(b)

Fig. 7.   (a) EELS from locations a, b, and c marked in Fig. 6(c). (b) Si - $L_{2,3}$ edges of the standard Si, $SiO_2$, and the interfacial amorphous oxide layer.

are contacted in air, the $OH^-$ molecules from air terminated on the surfaces react and produce water across the interface. The water can easily be diffused through $SiO_xN_y$ layer into bulk. This results in strong covalent bonds of Si-O-Si at the interface due to reactions between the highly reactive surfaces ($SiO_xN_y$) in SPAB.

## IV. CONCLUSION

The sequentially plasma-activated silicon surfaces have shown hydrophilic and highly reactive behavior. The bonding mechanism is not identical with the conventional hydrophilic bonding of silicon/silicon. While postbonding heating does not impact on bonding strength compared with that at room temperature, the HRTEM of the bonded interface shows water rearrangement. The water from the interface absorbs in bulk, resulting in a thinner amorphous silicon oxide layer up to 150 °C. Further heating of the SPAB-bonded wafers desorbs water from the bulk. The heating at 225 °C starts producing hillocks at the interface, which turns into voids at temperatures higher than 400 °C to absorb the gas of hydrogen produced from the desorbed water at the interface. The new and bigger voids due to hydrogen gas appear at 600 °C, and they start accumulating at 800 °C, resulting in bubbles due to the accumulation of voids at the preferential sites. The EELS measurements showed that no nitrogen was detected in silicon or the interfacial silicon oxide. The Si - $L_{2,3}$ edges from the amorphous silicon oxide were identical with those of the standard $SiO_2$ at the bonded interface.

## REFERENCES

[1] Y. T. Cheng, L. Lin, and K. Najafi, "Localized silicon fusion and eutectic bonding for MEMS fabrication and packaging," *J. Microelectromech. Syst.*, vol. 9, no. 1, pp. 3–8, Mar. 2000.
[2] N. Miki, X. Zhang, R. Khanna, A. A. Ayón, D. Ward, and S. M. Spearing, "Multi-stack silicon-direct wafer bonding for 3D MEMS manufacturing," *Sens. Actuators A, Phys.*, vol. 103, no. 1/2, pp. 194–201, Jan. 2003.
[3] S. Lai, H. Lin, and C. Hu, "Effect of surface treatment on wafer direct bonding process," *Mater. Chem. Phys.*, vol. 83, no. 2/3, pp. 265–272, Feb. 2004.
[4] W. K. Jeung, C. H. Lim, J. Yuan, and S. W. Park, "Wafer level package for image sensor module," in *Proc. DTIP MEMS MOEMS*, Apr. 2008, pp. 201–206.
[5] X. X. Zhang and J. P. Raskin, "Low-temperature wafer bonding: A study of void formation and influence on bonding strength," *J. Microelectromech. Syst.*, vol. 14, no. 2, pp. 368–382, Apr. 2005.
[6] D. Liang, A. W. Fang, H. Park, T. E. Reynolds, K. Warner, D. C. Oakley, and J. E. Bowers, "Low temperature, strong $SiO_2$-$SiO_2$ covalent wafer bonding for III–V compound semiconductors-to-silicon photonic integrated circuits," *J. Electron. Mater.*, vol. 37, no. 10, pp. 1552–1559, Oct. 2008.

[7] R. H. Esser, K. D. Hobart, and F. J. Kub, "Improved low-temperature Si–Si hydrophilic wafer bonding," *J. Electrochem. Soc.*, vol. 150, no. 3, pp. G228–G231, Mar. 2003.

[8] H. Moriceau, F. Rieutord, C. Morales, and A. M. Charvet, "Surface plasma treatments enabling low temperature direct bonding," *Microsyst. Technol.*, vol. 12, no. 5, pp. 378–382, Apr. 2006.

[9] R. Beneyton, F. Fournel, F. Rieutord, C. Morales, and H. Moriceau, "Effect of prebonding surface treatments on Si–Si direct bonding: Bonding void decrease," *ECS Trans.*, vol. 3, no. 6, pp. 239–248, 2006.

[10] Z. Tang, P. Peng, T. Shi, G. Liao, N. Lei, and S. Liu, "Effect of nanoscale surface topography on low temperature direct wafer bonding process with UV activation," *Sens. Actuators A, Phys.*, vol. 151, no. 1, pp. 81–86, Apr. 2009.

[11] X. Ma, W. Liu, and Z. Song, "Void-free low-temperature silicon direct-bonding technique using plasma activation," *J. Vac. Sci. Technol. B*, vol. 25, no. 1, pp. 229–234, Jan./Feb. 2007.

[12] T. Suni, K. Henttinen, A. Lipsanen, J. Dekker, H. Luoto, and M. Kulawski, "Wafer scale packaging of MEMS by using plasma-activated wafer bonding," *J. Electrochem. Soc.*, vol. 153, no. 1, pp. G78–G82, 2006.

[13] V. Dragoi, G. Mittendorfer, C. Thanner, and P. Lindner, "Wafer-level plasma activated bonding: New technology for MEMS fabrication," *Microsyst. Technol.*, vol. 14, no. 4/5, pp. 509–515, Apr. 2008.

[14] T. Suga, T. H. Kim, and M. M. R. Howlader, "Combined process for wafer direct bonding by means of the surface activation method," in *Proc. 54th IEEE ECTC*, 2004, pp. 484–490.

[15] M. M. R. Howlader, T. Suga, H. Itoh, and M. J. Kim, "Sequential plasma activated process for silicon direct bonding," *ECS Trans.*, vol. 3, no. 6, pp. 191–202, 2006.

[16] M. M. R. Howlader, S. Suehara, and T. Suga, "Room temperature wafer level glass/glass bonding," *Sens. Actuators A, Phys.*, vol. 127, no. 1, pp. 31–36, Feb. 2006.

[17] M. M. R. Howlader, S. Suehara, H. Takagi, T. H. Kim, R. Maeda, and T. Suga, "Room-temperature microfluidics packaging using sequential plasma activation process," *IEEE Trans. Adv. Packag.*, vol. 29, no. 3, pp. 448–456, Aug. 2006.

[18] Q. Y. Tong and U. Gösele, *Semiconductor Wafer Bonding*. New York: Wiley, 1999.

[19] M. Bruel, "Application of hydrogen ion beams to silicon on insulator material technology," *Nucl. Instrum. Methods Phys. Res. B, Beam Interact. Mater. At.*, vol. 108, no. 3, pp. 313–319, Feb. 1996.

[20] M. M. R. Howlader, T. Suga, H. Itoh, T. H. Lee, and M. J. Kim, "Role of heating on plasma-activated silicon wafers bonding," *J. Electrochem. Soc.*, vol. 156, no. 11, pp. H846–H851, 2009.

[21] M. Shimbo, K. Furukawa, K. Fukuda, and K. J. Tanzawa, "Silicon-to-silicon direct bonding method," *J. Appl. Phys.*, vol. 60, no. 8, pp. 2987–2989, Oct. 1986.

[22] S. W. Choi, W. B. Choi, Y. H. Lee, B. K. Ju, M. Y. Sung, and B. H. Kim, "The analysis of oxygen plasma pretreatment for improving anodic bonding," *J. Electrochem. Soc.*, vol. 149, no. 1, pp. G8–G11, Jan. 2002.

[23] C. Yang, U. Tartaglino, and B. N. J. Persson, "Influence of surface roughness on superhydrophobicity," *Phys. Rev. Lett.*, vol. 97, no. 11, pp. 116 103/1–116 103/4, Sep. 2006.

[24] M. G. Kibria, F. Zhang, T. H. Lee, M. J. Kim, and M. M. R. Howlader, "Comprehensive investigation of sequential plasma activated Si/Si bonded interface for nano-integration on wafer scale," *Nanotechnology*, vol. 21, no. 13, p. 134 011, Apr. 2010.

[25] S. N. Farrens, J. R. Dekker, J. K. Smith, and B. E. Roberds, "Chemical free room temperature wafer to wafer direct bonding," *J. Electrochem. Soc.*, vol. 142, no. 11, pp. 3949–3955, Nov. 1995.

[26] X. Ma, C. Chen, W. Liu, X. Liu, X. Du, Z. Song, and C. Lin, "Study of the Ge wafer surface hydrophilicity after low-temperature plasma activation," *J. Electrochem. Soc.*, vol. 156, no. 5, pp. H307–H310, May 2009.

[27] C. Wang, E. Higurashi, and T. Suga, "Void-free room-temperature silicon wafer direct bonding using sequential plasma activation," *Jpn. J. Appl. Phys.*, vol. 47, no. 4, pp. 2526–2530, Apr. 2008.

[28] S. Hayashi, R. Sandhu, M. Wojtowicz, Y. Sun, R. Hicks, and M. S. Goorsky, "Determination of wafer bonding mechanisms for plasma activated SiN films with X-ray reflectivity," *J. Phys. D, Appl. Phys.*, vol. 38, no. 10A, pp. A174–A178, May 2005.

[29] T. Sekiguchi, K. Kimoto, T. Aoyama, and Y. Mitsui, "Nitrogen distribution and chemical bonding state analyses in oxynitride film by spatially resolved electron energy loss spectroscopy (EELS)," *Jpn. J. Appl. Phys. 2, Lett.*, vol. 37, no. 6B, pp. L694–L696, Jun. 1998.

[30] M. M. R. Howlader, J. G. Wang, and M. J. Kim, "Influence of nitrogen microwave radicals on sequential plasma activated bonding," *Mater. Lett.*, vol. 64, no. 3, pp. 445–448, Feb. 2010.

**Matiar M. R. Howlader** received the B.Sc.Eng. degree in electrical and electronic engineering from Khulna University of Engineering and Technology, Khulna, Bangladesh, in 1988, and the M.S. and Ph.D. degrees in nuclear engineering from Kyushu University, Fukuoka, Japan, in 1996 and 1999, respectively.

From 2000 to 2005, he was with the Research Center for Advanced Science and Technology, The University of Tokyo, Tokyo, Japan, as an endowed Associate Professor. He is currently an Assistant Professor in the Department of Electrical and Computer Engineering, McMaster University, Hamilton, ON, Canada. His research focuses on the chip-size and wafer-level planar and vertical integration for microelectronics, microelectromechanical systems, and optoelectronics packaging, oxidation behavior of solders and electronic materials, interfacial adhesions, and radiation effects on materials and packages. He has started a new initiative on nanobonding and packaging of materials, devices, and components for microsystems and nanosystems for health and environmental applications. He has published over 40 refereed papers and over 65 international proceedings articles.

Dr. Howlader is a member of the Japan Institute of Electronic Packaging. He was the recipient of the Best Technical Paper Award at the International Conference on Electronic Packaging in 2003.

**G. Kagami** received the B.S. degree in electronics engineering and the M.S. degree in electronics and applied physics from Osaka Electro-Communication University, Osaka, Japan, in 1995 and 1997, respectively.

Since 1997, he has been with Shinko Seiki Company, Ltd., Kobe, Japan, working on plasma and deposition systems.
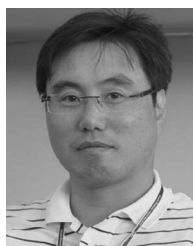
**Sang Ho Lee** received the B.S. degree in materials science and engineering from Korea Advanced Institute of Science and Technology, Daejeon, Korea, in 1991, and the Ph.D. degree in materials science and engineering from the University of California, Los Angeles, in 2004.

He is currently a Research Scholar at the University of Texas at Dallas, Richardson. His recent work has focused on developing transparent oxide semiconductors and *in situ* plasma diagnostic systems.

**Jinguo G. Wang** received the Ph.D. degree in materials science and engineering from the University of Science and Technology Beijing, Beijing, China, in 1994.

He was a Postdoctoral Scholar at Lawrence Livermore National Laboratory from 1997 to 1999 and at the University of California, Irvine, from 1999 to 2000, where he worked on high-temperature deformation of intermetallic alloys, as well as transmission electron microscopy. From 2000 to 2006, he was with the Materials Research Institute, The Pennsylvania State University, University Park, as a Research Associate and the Manager of the TEM facility. He is currently an Associate Director of the Nanocharacterization Facility, University of Texas at Dallas, Richardson. He has published 90 technical papers and over 40 international proceedings articles. His research focuses on HRTEM, STEM, EDS, EELS, nanostructured materials, and nanoelectronics.

Dr. Wang is a member of the Materials Research Society and the Microscopy Society of America.

**Moon J. Kim** received the B.S., M.S., and Ph.D. degrees in materials science from Arizona State University, Phoenix, in 1984, 1986, and 1988, respectively.

He is currently a Professor in the Department of Materials Science and Engineering, University of Texas at Dallas (UTD), Richardson. He is also an Adjunct Professor in the Simmons Comprehensive Cancer Center, UT Southwestern Medical Center, Dallas, TX. He is currently the Director of UTD's Nano-Characterization Facility, Future Semiconductor Innovation and Commercialization consortium, and Silicon Wafer Engineering and Defect Science Industry University Collaborative Research Center. His expertise includes high-resolution electron microscopy, heterogeneous materials integration by wafer bonding, and 3-D functional nanostructure fabrication. He has authored or coauthored over 210 refereed papers. His primary research focus is nanofabrication, manipulation, and characterization of materials for nanoelectronics and functional 3-D nanostructured system applications.

**Akira Yamauchi** graduated from the Precision Engineering Department, School of Engineering, Shizuoka University, Shizuoka, Japan, in 1983.

He established Bondtech Company, Ltd., Kyoto, Japan, five years ago, and successfully achieved bonding on the submicron scale at the wafer level by suggesting a low-temperature bonding process characterized by ultrahigh-precision alignment technology. As an equipment manufacturer, he has developed the surface-activation-based nanobonding and interconnect system equipment as a joint research collaboration with Prof. M. Howlader of McMaster University, Hamilton, ON, Canada, and Prof. T. Suga of The University of Tokyo, Tokyo, Japan. He has also developed this technology in the field of MEMS and 3-D LSI, and has been developing equipment and proposing processes adapted to C2C, C2W, and WOW.